

Cu(II) and Zn(II) complexes with unsymmetrical tetradentate Schiff base ligands: Synthesis, spectral characterization, antimicrobial assay and DNA binding property

Natarajan Raman^{1,*}, Abraham Selvan², Rajkumar Mahalakshmi¹, Muthusamy Selvaganapathy¹

¹Research Department of Chemistry, VHNSN College, Virudhunagar-626 001, India

²Department of Chemistry, Veltech Hightech, Engineering College, Avadi, India

* E-mail: drn_raman@yahoo.co.in

Received 14 December 2011

Received in revised form 18 September 2012

Accepted 21 September 2012

The reaction of copper(II) chloride and zinc(II) chloride with N-(2-methylphenyl)-3-(1'-salicylaldehyde-2'-imine-ethane)-butanamide(H2L2a) or (MPSB), N-(2-methylphenyl)-3-(1'-(3'-methoxysalicylaldehyde-2'-imine-ethane)-butanamide (H2L2b) or (MPMSB) and N-(2-methylphenyl)-3-(1'-(2'-hydroxyacetylene-2'-imine-ethane)-butanamide (H2L2c) (MPHB) leads to the formation of a series of new complexes and they have been characterized by the spectral and analytical techniques. For the complexes [CuL2a-c] and [ZnL2a-c], the central metal ion is coordinated to two azomethine nitrogen atoms and one phenolic oxygen atom of the aromatic aldehydes as well as 2-hydroxyacetophenone and enolic oxygen atom of the 2'-methylacetoacetanilide. DNA binding studies reveal the stronger binding capability of the present copper(II) complexes, confirmed by the absorbance, cyclic voltammetry, differential pulse voltammogram and viscometric studies. Similarly, remaining complexes do the same in the ligand field with less binding constants. In addition, fungistatic and bacteriostatic activities of both ligands and complexes have been evaluated. copper(II) complexes have shown the most significant activities.

Keywords: Schiff base; Copper complexes; DNA binding; Cyclic voltammetry; Viscometry

1. INTRODUCTION

The Schiff base ligands derived from the reaction of salicylaldehyde / substituted salicylaldehyde with diamines have been extensively studied. The metal complexes of 2'-methylacetoacetanilide and its derivatives have been reported to show interesting biochemical properties such as antitumour, antioxidant and antimicrobial activities [1]. The bacterial and fungicidal activities of transition metal complexes are due to their ability to form chelates with the essential metal ions bond through nitrogen as well as oxygen donor atom of ligand.

Redox-active transition metal complexes that stabilize various oxidation states of the metal centers are of considerable interest because of their potential significance as model of redox metalloenzymes and as effective redox reactants or catalysts [2]. Furthermore, a recently emerged field of research concerns the use of redox-active metal complexes such as Cu(II) complexes with salen and related Schiff bases as synthetic chemical nucleases or DNA damaging agents . For a specific metal ion, the main factors which are the nature and the arrangement of the donor atoms around the metal bonding site or the nature and the position of substituents, determine redox properties. Among various ligands, many Schiff bases derived from salicylaldehyde, 2-hydroxy

acetophenone and related aromatic aldehydes have been found to stabilize copper(I) with the Cu(II)/Cu(I) redox process.

Based on the literature [3], we have synthesized monocondensation Schiff bases of L1a by using diamine (e.g. ethylenediamine) and salicylaldehyde. This intends us to design and synthesize the monocondensation Schiff bases L1b and L1c. These monocondensation Schiff bases further react with 2'-methylacetoactanilide and put forward us to discuss the effect of substituents on their biological studies. Herein, we report the synthesis, spectral characterization, DNA binding activities and antimicrobial studies of metal complexes of new Schiff base derivatives, MPSB, MPMSB and MPHB.

2. EXPERIMENTAL

2.1. General Materials

2'-methylacetoactanilide was purchased from Aldrich Chemical Co. Ethidium bromide (EB), calf thymus DNA (CT DNA) and pBR322 plasmid DNA were purchased from Sigma. All other chemicals used were of analytical grade. Solvents were dried and distilled before use according to standard procedures. All the experiments involved with the interaction of the ligands and their metal complexes with CT DNA were carried out in doubly distilled water buffer containing 5 mM Tris [Tris(hydroxymethyl)-aminomethane] and 50 mM NaCl and adjusted to pH 7.2 with hydrochloric acid. Solution of CT DNA in Tris-HCl buffer gave ratio of UV absorbance of about 1.8–1.9:1 at 260 and 280 nm, indicating that the CT DNA was sufficiently free of protein. The CT DNA concentration per nucleotide was determined spectrophotometrically by employing an extinction coefficient of $6600 \text{ M}^{-1}\text{cm}^{-1}$ at 260 nm [4].

2.2. Instrumentation

UV-Vis. spectra were recorded on a Shimadzu Model 1601 UV-Visible Spectrophotometer. IR spectra of the ligand and its metal complexes were recorded on a Perkin-Elmer FTIR-1605 spectrophotometer using KBr discs. ^1H NMR spectra were measured at room temperature on a Bruker Avance DRX 300 FT-NMR spectrometer using tetramethylsilane as the internal standard. The complexes were analyzed for their metal contents, following standard procedures [5] after decomposition with a mixture of conc. HNO_3 and HCl, followed by conc. H_2SO_4 . Microanalyses (C, H, N) were carried out on a Perkin-Elmer 240 elemental analyzer. Mass spectrometry experiments were performed on a JEOL-AccuTOF JMS-T100LC mass spectrometer equipped with a custom-made electrospray interface (ESI). The X-band EPR spectra of the complexes were recorded at RT (300 K) and LNT (77 K) using DPPH as the g-marker. X-ray diffraction experiments were carried out on XPERT-PRO diffractometer system. Copper $\text{K}\alpha_1$ line, with wavelength of 1.5406 \AA generated with a setting of 30 mA and 40 kV with the electrodes was used for diffraction. The slit width setting was 91 mm. The diffracting angle (2θ) was scanned from 10.0881 to 79.9381 continuously with a rate of 2° per minute. The whole process took place at a temperature of 25°C . Room temperature magnetic susceptibility measurements were carried out on a modified Gouy-type magnetic balance, Hertz SG8-5HJ. The molar conductivity of the complexes in DMF solution (10^{-3} M) was measured using a conductometer model 601/602. Voltammetric experiments were performed on a CHI 620C electrochemical analyzer in freshly distilled DMF solution.

2.3. Methodology for Antimicrobial Activity

The antimicrobial activities were carried out by disk diffusion technique [6]. Nutrient agar was melted at 45°C and inoculated by the cell suspension bacteria or yeast. The flask was shaken

well and poured into a petri-disk. Filter paper disks (Whatman No.2) were thoroughly moistened by antibiotics (50 µg) and the discs were aseptically transferred and placed upon the surface of the inoculated plates with tested organisms and kept in incubator at 37 °C for 24 h in case of bacteria and at 28 °C for 48 h in case of fungi. Minimum Inhibitory Concentrations (MIC's) were determined by the microdilution broth method [7]. The minimum inhibitory concentration was determined by assaying at concentration of compounds along with standards at the same concentration. MIC is the lowest concentration of an antimicrobial compound that will inhibit the visible growth of microorganisms after overnight incubation.

2.4. Methodology for DNA Binding Analysis

Electronic Spectra: In absorption studies the complex was dissolved in DMF to get the desired concentration. The spectroscopic titrations were carried out by adding increasing amounts of DNA to a solution of the complex at a fixed concentration contained in a quartz cell. The UV–Vis spectra were recorded after equilibration at 20 °C for 10 min after each addition. The titration processes were repeated until there was no change in the spectra, indicating binding saturation had been achieved. The intrinsic binding constant K_b was determined from the plot of $[DNA]/(\epsilon_a - \epsilon_f)$ vs. $[DNA]$ according to the following equation (1):

$$[DNA]/(\epsilon_a - \epsilon_f) = [DNA]/(\epsilon_b - \epsilon_f) + 1/[K_b(\epsilon_b - \epsilon_f)] \text{ ----- (1)}$$

where $[DNA]$ is the concentration of DNA in base pairs, the apparent absorption coefficients ϵ_a , ϵ_f and ϵ_b correspond to $A_{obs}/[complex]$, extinction coefficient for the free complex and the extinction coefficient of the complex in the totally bound form, respectively. The data were fitted to Eq. (1), with a slope equal to $1/(\epsilon_b - \epsilon_f)$ and y-intercept equal to $1/[K_b(\epsilon_b - \epsilon_f)]$ and K_b was obtained from the ratio of the slope to the intercept.

Cyclic Voltammetry: The cyclic voltammograms of synthetic compounds were recorded at room temperature (25 °C) in DMF solution. An assembly of three electrodes consists of glassy carbon working electrode, a platinum wire auxiliary electrode and Ag/AgCl reference electrode was used and tetrabutylammonium perchlorate (TBAP) with 0.1 M concentration as supporting electrolyte. The working electrode was cleaned after every electrochemical assay. All the solutions examined by electrochemical techniques were purged with nitrogen for 10 min prior to each set of experiments.

The difference between forward and backward peak potentials can provide a rough evaluation of the degree of the reversibility of one electron transfer reaction. The analysis of cyclic voltammetric responses with the scan rate varying from 50 to 250 mVs⁻¹ gives the evidence for a quasi-reversible one electron oxidation. The decreased extents of the peak currents observed for all metal(II) complexes upon addition of CT DNA indicate that complexes interact with DNA through binding mode. The Nernst equation (Eq. 2) can be used to estimate the ratio of equilibrium constants for the binding of the oxidative and reductive ions to DNA.

$$E_b^\circ - E_f^\circ = 0.0591 \log(K_{red}/K_{ox}) \text{ ----- (2)}$$

where E_b° and E_f° are the formal potentials of the bound and free complex forms, K_{red} and K_{ox} are the corresponding binding constants for the binding of reduction and oxidation species to CT DNA, respectively. The drop of the voltammetry currents in the presence of DNA may be attributed to slow diffusion of the metal complex bound to CT DNA. This in turn indicates the extent of binding affinity of the complex to DNA.

Viscosity Measurements: These were performed using an Ubbelodhe viscometer, immersed in a thermostatic water-bath that maintained at a constant temperature at 25.0 ± 0.1 °C. Different amounts of complex were then added into the viscometer while keeping the DNA concentration constant. The flow time of each sample was measured by a digital stopwatch for three times and an

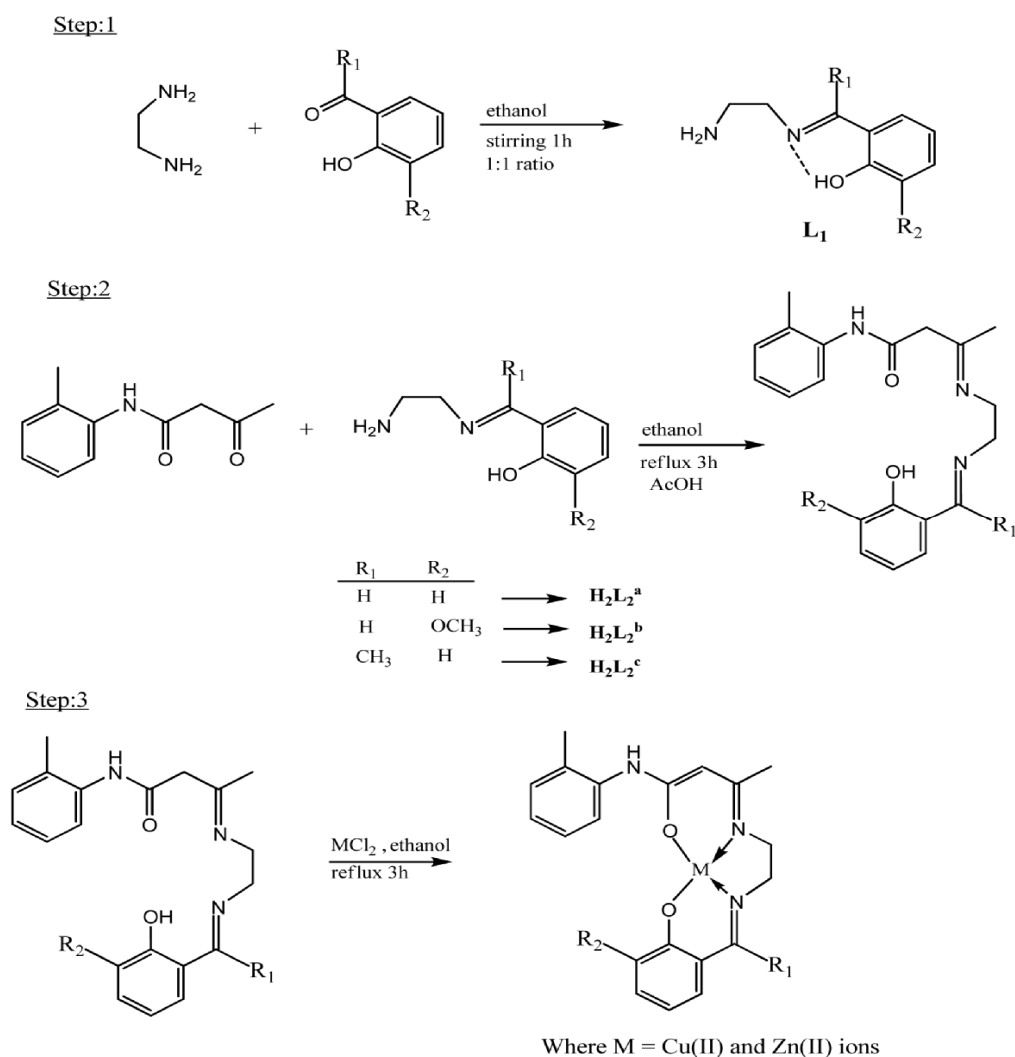
average one was calculated. The values of relative specific viscosity $(\eta/\eta_0)^{1/3}$ versus $[\text{complex}]/[\text{DNA}]$ ratio, where η and η_0 are the viscosity of DNA in the presence and absence of the complex, respectively.

2.5. General Procedure for Synthesis of Ligands L_1^a , L_1^b and L_1^c

Synthesis and Characterization of Ligands L_1^a , L_1^b and L_1^c are presented in supplementary material.

2.5.1. Synthesis of Ligands $H_2L_2^a$, $H_2L_2^b$ and $H_2L_2^c$

Hot solution of 2'-methylacetoacetanilide (1.39 g, 10 mmol) in 25 mL ethanol was mixed with hot solution of L_1^a , L_1^b and L_1^c (1.64, 1.94 and 1.78 g, 10 mmol, respectively) and the reaction mixture was left under reflux for 3 h. The formed solid product was separated by filtration, purified by crystallization from ethanol, washed with ether and dried in a vacuum over anhydrous calcium chloride. General formulae of the ligands are shown in scheme 1.



Scheme 1. Synthetic steps for metal complexes.

2.6. Synthesis of Metal Complexes

An ethanolic hot solution of Cu(II)/Zn(II) chloride (0.170 g/0.136 g, 1 mmol) was mixed to the hot solution of appropriate Schiff base ligands $\text{H}_2\text{L}_2^{\text{a}}$ / $\text{H}_2\text{L}_2^{\text{b}}$ / $\text{H}_2\text{L}_2^{\text{c}}$ (0.3374/ 0.3674/ 0.3514 g respectively, 1 mmol) in the same solvent (25 mL) in 1:1 molar ratio. The resulting mixture was refluxed for 3 h whereupon the complexes precipitated. They were collected by filtration, washed several times with ethanol followed by ether and dried under vacuum over CaCl_2 .

3. RESULTS AND DISCUSSION

3.1. Chemistry

The general chemistry of the synthesized complexes is discussed in supplementary material.

3.2. IR Spectra

The IR spectra of the metal complexes are similar to each other, except for slight shifts and intensity changes of few vibration peaks caused by different metal(II) ions, which indicate that the metal complexes have similar structure. Careful examining of the IR spectra of the complexes and comparison with that of the ligands one may conclude the following observations:

(i) The lower value of $\nu(\text{C}=\text{N})$ stretching on complexation may be explained on the basis of a drift of lone pair density of azomethine nitrogen towards the metal atom indicating that coordination takes place through nitrogen of (C=N) groups. The appearance of a new band at 397–422 cm^{-1} is due to $\nu(\text{M}-\text{N})$ vibration; the wide range may be due to a relatively strong bond with the metal ion.

(ii) In all the Schiff base complexes, the $\nu(\text{C}=\text{O})$ band disappeared; the appearance of $\nu(\text{C}=\text{N})$ band is slightly shifted to lower frequency at 1584–1604 indicating co-ordination of the Schiff bases through the azomethine nitrogen atom [8]. A strong band which appeared in the spectra of the ligands around 1618–1633 cm^{-1} range due to $\nu(\text{C}-\text{O})$ completely disappeared on complexation. This may be due to the enolisation and subsequent coordination through the deprotonated oxygen atom [9]. The above interpretation is further supported by the appearance of the non-ligand bands at 452–520 cm^{-1} , assigned to $\nu(\text{M}-\text{O})$ [10].

(iii) All the ligands also display bands at 1276, 1276 and 1268 cm^{-1} which are assigned to phenolic C–O stretching vibrations for $\text{H}_2\text{L}_2^{\text{a}}$, $\text{H}_2\text{L}_2^{\text{b}}$ and $\text{H}_2\text{L}_2^{\text{c}}$, respectively. These bands are strongly affected by chelation through the phenolic–CO groups of the above ligands and the shift to lower frequency range 1218–1248 cm^{-1} after complexation in all metal complexes, suggesting that the phenolic oxygen participates in the coordination mode [11]. This has been further supported by the disappearance of the broad $\nu(\text{OH})$ peak around 3265–3483 cm^{-1} in all the metal complexes, indicating deprotonation of the phenolic proton prior to coordination [12].

3.3. Electronic Spectra and Magnetic Moments

Electronic spectral data and magnetic susceptibility measurements have been used to establish the geometry of the Cu(II) and Zn(II) metal complexes, recorded in the 200–1100 nm range in DMF. These data along with the tentative assignments are presented in experimental part. In the electronic spectra of the ligands and its mononuclear metal complexes, the wide range bands were observed due to either the $\pi \rightarrow \pi^*$ and $n \rightarrow \pi^*$ of C=N chromophore or charge-transfer transition arising from π -electron interactions between the metal and ligand, which involves either a metal-to-ligand or ligand-to-metal electron transfer.

The electronic spectra of the free ligands in DMF showed strong absorption bands in the ultraviolet region that could be attributed respectively to the $\pi \rightarrow \pi^*$ and $n \rightarrow \pi^*$ transitions in the benzene ring or azomethine (–C=N) groups for free ligands. In the electronic spectra of the metal

complexes, the band of the high or low wavelength side shows an inequable bathochromic or hypsochromic shifts relative to their free ligands. The absorption bands between 230 and 365 nm in free ligands change a bit in intensity and remain essentially slightly changed for metal complexes. The absorption shift and intensity change in the spectra of the metal complexes most likely originate from the metalation which increases the conjugation and delocalization of the whole electronic system and results in the energy change of the $\pi \rightarrow \pi^*$ and $n \rightarrow \pi^*$ transition of the conjugated chromophore [16]. The results clearly indicate that the ligand coordinates to Cu(II) and Zn(II) ions, which are in accordance with the results of the other spectral data. Furthermore, in the case of the Cu(II) complexes, the absorption bands in the visible region are observed at between 500 and 625 nm for Cu(II) complexes as low intensity bands. These bands are considered to arise from the forbidden d-d transition, which is generally too weak.

The broad band centered at 507-625 nm for the copper(II) complexes of all ligands and their magnetic moment values strongly support a square-planar geometry ($^2B_{1g} \rightarrow ^2A_{1g}$) around the metal ion [17]. The bands at 260-387 nm can be assigned to a CT band from filled orbitals Cu(II) to the anti-bonding π^* orbitals of the ligands.

The zinc(II) complexes are found to be diamagnetic. By analogy with those described for the complexes containing N,O donor Schiff bases, the electronic spectral data and empirical formulae of the zinc(II) complexes are consistent with a tetrahedral geometry around the metal ion [18,19].

3.4. ^1H NMR spectra

The chemical shifts of the different type of protons of the ligands $\text{H}_2\text{L}_2^{\text{a}}$, $\text{H}_2\text{L}_2^{\text{b}}$ and $\text{H}_2\text{L}_2^{\text{c}}$ and their diamagnetic Zn(II) complexes are listed in experimental part. The ligands displayed the signals at 3.81-3.91 and 9.47-9.82 ppm which can be attributed to amide proton Ph-NH-, and phenolic-OH protons respectively [13]. In addition to this, a set of multiplet was observed in the range 6.64-7.77 ppm due to the presence of aromatic protons. In the spectra of the Zn(II) complexes of $\text{H}_2\text{L}_2^{\text{a}}$, $\text{H}_2\text{L}_2^{\text{b}}$ ligands, signals due to the hydrogen atom of the azomethine group of the ligands shifted to the downfield. This shows that the nitrogen atom of the azomethine group is coordinated to the metal ions [14]. The OH signals observed for the ligands had disappeared confirming that the phenolic C-OH group is coordinated to the transition metal ions. The enolic nature of all Schiff base ligands shows broad singlet at 13.92-14.13 ppm, due to rapid exchange interaction of keto-enol tautomerism [15].

3.5. Mass Spectral Studies

In the present investigation, the mass spectrum of $\text{H}_2\text{L}_2^{\text{a}}$ showed the formation of molecular ion peak at $m/z = 337$, which corresponds to the total molecular weight of the ligand and also exhibited two additional peaks at 335 and 338 m/z , corresponding to (M-2) and (M+1) peaks respectively. Apart from this, the spectrum showed few peaks at 108, 117 (M-1), 189 (M-1), 148, 217, 231 (M-1), 245, 285 (M-1) and 298, may be due to different fragments $[\text{C}_7\text{H}_{10}\text{N}]^+$, $[\text{C}_8\text{H}_8\text{N}]^+$, $[\text{C}_{11}\text{H}_{14}\text{N}_2\text{O}]^+$, $[\text{C}_9\text{H}_{10}\text{NO}]^+$, $[\text{C}_{13}\text{H}_{17}\text{N}_2\text{O}]^+$, $[\text{C}_{13}\text{H}_{16}\text{N}_2\text{O}_2]^+$, $[\text{C}_{14}\text{H}_{19}\text{N}_3\text{O}]^+$, $[\text{C}_{16}\text{H}_{20}\text{N}_3\text{O}_2]^+$ and $[\text{C}_{17}\text{H}_{20}\text{N}_3\text{O}_2]^+$ respectively. $\text{H}_2\text{L}_2^{\text{a}}$ showed one additional fragment at $m/z = 271$, which corresponds to $[\text{C}_{16}\text{H}_{21}\text{N}_3\text{O}]^+$ and also exhibited two additional peaks at 270 and 269 m/z , corresponding to (M-1) and (M-2) peaks respectively. The ESI mass spectrum of **1** shows the molecular ion peak at $m/z = 398$, which is due to $[\text{C}_{20}\text{H}_{21}\text{N}_3\text{O}_2\text{Cu}]^+$ supporting the composition of the complexes as metal: ligand ratio (1:1) according to the elemental analyses. Complex **1** also exhibits few peaks at 335, 317, 216 and 189(M-1) may be due to different fragments $[\text{C}_{20}\text{H}_{21}\text{N}_3\text{O}_2]^+$, $[\text{C}_{18}\text{H}_{21}\text{N}_3\text{O}_2]^+$, $[\text{C}_{13}\text{H}_{16}\text{N}_2\text{O}]^+$ and $[\text{C}_{11}\text{H}_{13}\text{N}_2\text{O}]^+$ respectively.

3.6. EPR Spectroscopy

Copper(II) with a d^9 electron configuration is well suited to be studied by EPR spectroscopy. The X-band EPR spectrum of the copper(II) complex (Fig. 1) was recorded in the solid state at room temperature and in DMSO at the temperature of liquid nitrogen using DPPH free radical as the 'g' marker. As expected, the room temperature powder spectra of the complexes are very broad due to dipolar effects and thus, do not give detailed information about the nature of the complexes and so no further discussion has been presented. The room temperature solution spectrum of **1** in dimethylsulphoxide shows a normal four line isotropic spectrum and simulation of the spectrum permitted to evaluate the spin Hamiltonian parameters, g_{iso} and A_{iso} , as 2.20 and 216 respectively. The hyperfine structure quartet due to the coupling with the nuclear spin of the copper ($I = 3/2$) is well resolved in the parallel part (lower field) corresponding to the electron spin – nuclear spin interaction as well as the super hyperfine structure due to the coupling with the two nitrogen atoms ($N, I = 1$). The perpendicular part is only poorly resolved because of some overlap at X-band frequencies.

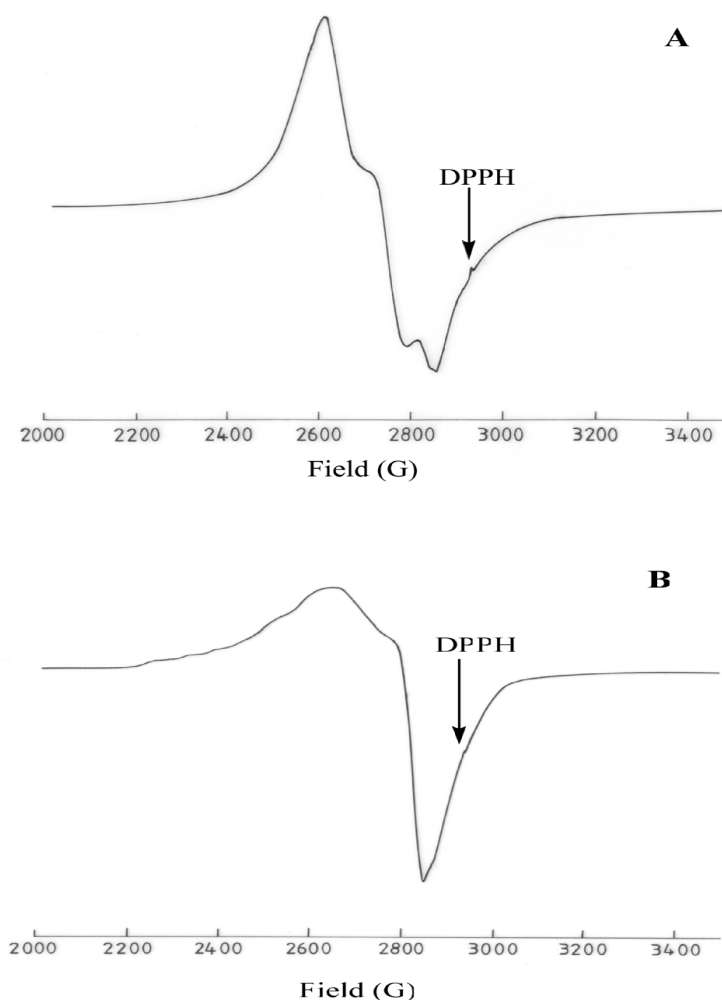


Fig. 1. EPR spectrum of complex **1** at A) RT (300 K) and B) LNT (77 K).

The g tensor values of Cu(II) complexes can be used to derive the ground state. In square-planar complexes the unpaired electron lies in the $d_{x^2-y^2}$ orbital giving $^2B_{1g}$ as the ground state with the $g_{||} > g_{\perp} > g_e$ (2.0027) [20]. The $g_{||}$ and g_{\perp} values determined from the EPR spectra of the

complex **1** recorded in microcrystalline powder at room temperature (2.33 and 2.14) suggest that the unpaired electron is localized in the $d_{x^2-y^2}$ orbital of the Cu(II) ion and are characteristic for the axial symmetry.

These data are in good agreement with those obtained from the electronic spectra and confirm the square-planar geometry for complex **1**. The hyperfine structure observed corresponds to N_2O_2 coordination mode in square-planar complexes [21]. From the values of the g factors it may be determined the geometric parameter G , representing a measure of the exchange interaction between the Cu(II) centers in polycrystalline compound following the formula $G = (g_{\parallel} - 2)/(g_{\perp} - 2)$. If $G < 4$, it is considered the existence of some exchange interactions between the Cu(II) centers and if $G > 4$, the exchange interactions are neglected. Thus, in case of complex **1**, the axial symmetry parameter $G = 2.38$ which is less than 4.0 indicates considerable exchange interaction between metal ions [22].

It has been reported that g_{\parallel} values are sensitive to the covalent nature of the metal–ligand bond; the values above 2.3 show ionic character and lower values reveal covalent character [23]. The present EPR results show that g_{\parallel} is higher than 2.3 in this case suggesting that the copper complex is ionic in nature. They also show that g_{\parallel} is 2.33, which is in conformity with the presence of mixed copper–nitrogen and copper–oxygen bonds in these chelates. The empirical ratio $g_{\parallel}/A_{\parallel}$ is frequently used to evaluate distortions in tetra coordinated copper(II) complexes [24]. The ratio close to 100, indicates a roughly square planar structure around the copper(II) ion [25] and the values from 170 to 250 are indicative of a distorted tetrahedral geometry. The present value of the $g_{\parallel}/A_{\parallel}$ ratio for complex **1** is 93 indicating nearly square-planar environments around the Cu(II) ion with small distortions.

The EPR parameters g_{\parallel} , g_{\perp} , A_{\parallel} and the energies of d–d transition were used to evaluate the bonding parameters α^2 , β^2 , δ^2 which may be regarded as measures of the covalency of the in-plane σ bonds, in-plane π bonds and out-of-plane π bonds. It is clear that in-plane σ -bonding (1.12) is less covalent than in-plane π -bonding (0.81). By examining the trend of the α^2 and β^2 values obtained, it can be seen that the less covalent character in the Cu(II) complex satisfactorily correlates with electron density at the nitrogen donor atom. The orbital reduction factors K_{\parallel} and K_{\perp} were calculated using the expressions reported elsewhere [26]. Likewise, according to Hathaway, for pure σ bonding, $K_{\parallel} \approx K_{\perp} \approx 0.77$, for in-plane π bonding, $K_{\parallel} < K_{\perp}$, and for out-of-plane π bonding, $K_{\parallel} > K_{\perp}$. The K_{\parallel} , K_{\perp} values, in complex **1**, are in agreement with the relation K_{\parallel} (0.91) $<$ K_{\perp} (1.53) which indicates the presence in-plane π bonding. The parameter K is a Fermi contact hyperfine interaction and is a measure of the contribution of s-electrons to the hyperfine interaction (value ≈ 0.30). For the complex **1**, the K (0.29) values obtained are in agreement with those estimated.

3.7. X-ray Powder Diffraction

Single crystal X-ray crystallographic investigation is the most precise source of information regarding the structure of the complexes, but the difficulty of obtaining crystalline complexes in proper symmetric form has rendered the powder X-ray diffraction method for such study. Powder XRD pattern of the Schiff base complexes were recorded over the $2\theta = 0-80^\circ$ range and complexes **1** and **2** are shown in Fig. 2 A and B. The trend of the curves decreases from maximum to minimum intensity indicating that these complexes are amorphous in nature in the present metal–ligand formation.

The diffractogram of **1** records 8 reflections between 10° and 80° (2θ) with maximum at $2\theta = 32.543^\circ$ corresponding to value of $d = 2.7492 \text{ \AA}$ (Table S1, presented in supplementary material). However, the diffractogram of **2** consists of 10 reflections with maxima at $2\theta = 32.648^\circ$ corresponding to value of $d = 2.7405 \text{ \AA}$ (Table S2, presented in supplementary material). The main peaks of **1** and **2** have been indexed using computer software by trial and error method, keeping in mind the characteristics of various symmetry systems until good fit could be obtained between

observed and calculated 2θ and $\sin^2\theta$ values. The method also yielded hkl (Miller indices) values. The relative intensities corresponding to prominent peaks have also been measured.

Table S1. X-ray diffraction data of complex 1.

2θ (Cal.)	2θ (Obser.)	$\sin^2\theta$ (Cal.)	$\sin^2\theta$ (Obser.)	d(A°) (Cal.)	d(A°) (Obser.)	h k l	Intensity (%)
16.493	16.746	0.0205	0.0212	5.3704	5.2900	0 2 0	65.36
22.293	22.887	0.0373	0.0393	3.9877	3.8825	2 1 2	23.77
28.689	28.644	0.0614	0.0612	3.1116	3.1139	2 0 4	11.35
32.543	32.808	0.0785	0.0797	2.7492	2.7275	3 2 1	100.00
33.271	33.232	0.0819	0.0817	2.6906	2.6937	2 3 2	90.34
40.531	40.710	0.1199	0.1209	2.2257	2.2145	0 4 4	10.14
68.233	68.160	0.3145	0.3139	1.3745	1.3746	4 5 6	16.63
76.025	76.542	0.3792	0.3836	1.2508	1.2436	7 2 5	20.29

Table S2. X-ray diffraction data of complex 2.

2θ (Cal.)	2θ (Obser.)	$\sin^2\theta$ (Cal.)	$\sin^2\theta$ (Obser.)	d(A°) (Cal.)	d(A°) (Obser.)	h k l	Intensity (%)
16.214	16.746	0.0198	0.0212	5.4669	5.2900	0 2 0	36.48
22.972	22.887	0.0396	0.0393	3.8682	3.8825	2 1 2	12.26
32.648	32.808	0.0789	0.0797	2.7405	2.7275	3 2 1	100.00
33.357	33.363	0.0823	0.0824	2.6839	2.6835	2 2 4	19.19
40.437	40.710	0.1194	0.1209	2.2307	2.2145	0 4 4	7.14
45.601	45.573	0.1501	0.1500	1.9893	1.9889	0 1 8	5.41
46.817	46.941	0.1578	0.1586	1.9388	1.9340	5 0 1	12.20
47.853	47.767	0.1644	0.1639	1.8993	1.9025	5 1 1	8.41
58.204	58.525	0.2365	0.2389	1.5837	1.5758	2 5 6	8.34
68.324	68.160	0.3153	0.3139	1.3717	1.3746	4 5 6	5.35

The structure of **1** yields values for lattice constant $a = 9.743 \text{ \AA}$, $b = 10.585 \text{ \AA}$, $c = 23.570 \text{ \AA}$ and unit cell volume $V = 2430.76 \text{ \AA}^3$. However the structure of **2** yields values for lattice constant $a = 9.743 \text{ \AA}$, $b = 10.585 \text{ \AA}$, $c = 19.611 \text{ \AA}$ and unit cell volume $V = 2022.47 \text{ \AA}^3$. In conjugation with these lattice parameters the condition [27] such as $a \neq b \neq c$ and of $\alpha = \beta = \gamma = 90^\circ$ required for the samples to be orthorhombic were tested and found to be satisfactory.

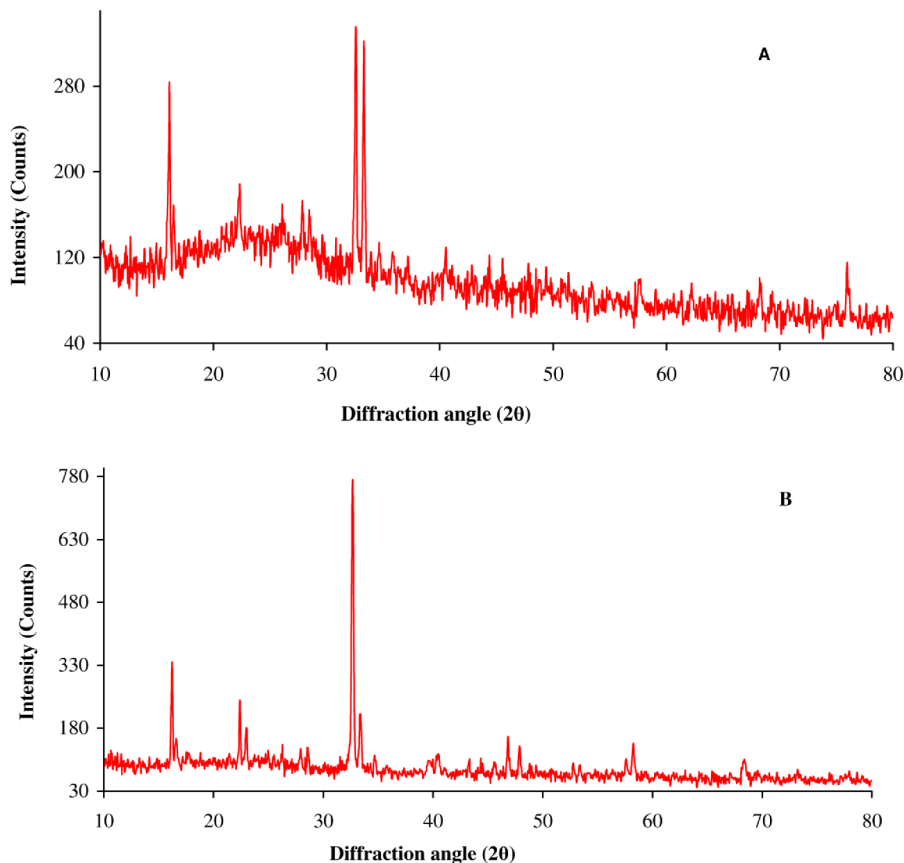


Fig. 2. Powder X-ray diffraction pattern of A) **1** and B) **2** complexes.

3.8. Pharmacology Results

3.8.1. Antibacterial Activity

All the synthesized compounds were screened for their antibacterial activity. All the tested complexes possessed variable antibacterial activity against both Gram-positive (*S. aureus* and *B. subtilis*) and Gram-negative (*P. aeruginosa* and, *E. coli*) bacteria. To compare the antibacterial activities shown by the synthesized complexes, standard drug namely Streptomycin was used (Table 1).

By careful study of the obtained results, we can see that the ligands have a weak action on all the tested microorganisms. The activity of MPSB, MPMSB and MPH B becomes more pronounced when coordinated to the metal ions. The compounds **2** and **5** could show very good efficacy on all clinical resistant strains, because of presence of methoxy group. All metal ions have varying antibacterial influence on bacterial species. The action of the tested complexes on Gram-negative bacteria is better than that on Gram-positive bacteria. The complexes **2** and **3** have more antibacterial active against *P. aeruginosa*. Complex **1** is more active against *E.coli* than **2** and **3**, but

less antibacterial active on *S.aureus* and *B.subtilis*. The antibacterial activity of the complexes is governed by the following factors: the chelate effect of the ligand; the nature of the donor atoms; the total charge on the complex ion; the nature of the metal ions and the geometrical structure of the complex. Since all the complexes have the same donating atoms (N, O), containing metals with the same oxidation state (M^{2+}), which form 5- or 6-membered chelating rings with ligand, therefore the more effective factors that influence the antibacterial activity are the geometrical shape and the nature of the central atoms. Besides from this many other factors such as solubility, dipole moment, conductivity influenced by metal ion may be possible reasons for remarkable antibacterial activities of these complexes [28].

Table 1. Antimicrobial activity expressed ($\mu\text{g/mL}$) as MIC of complexes and ligands on the positive and negative bacteria and fungal strains.

Complex	Antibacterial activity				Antifungal activity			
	<i>S. aureus</i>	<i>B. subtilis</i>	<i>E. coli</i>	<i>P. aeruginosa</i>	<i>A. niger</i>	<i>R. stolonifer</i>	<i>C. albicans</i>	<i>R. bataicola</i>
MPSB	19.36	21.04	18.64	17.28	16.21	19.74	15.52	19.28
MPMSB	20.41	19.73	16.37	15.75	14.72	17.49	14.58	17.12
MPHB	19.61	18.09	17.61	15.94	16.27	17.51	15.42	19.35
1	9.27	9.61	7.42	7.56	8.72	8.52	7.60	8.16
2	8.53	9.11	8.07	7.41	7.13	6.73	7.14	6.43
3	9.18	8.76	8.23	7.35	8.21	8.47	7.58	8.15
4	10.24	9.38	7.56	8.61	7.86	7.57	8.23	7.67
5	9.08	8.77	7.13	8.49	6.94	6.83	7.58	7.01
6	9.74	8.91	8.04	7.99	7.87	8.45	7.93	8.14
Streptomycin	1.98	2.32	1.04	1.16	----	----	----	----
Nystatin	----	----	----	----	1.82	2.35	2.18	1.96

Generally the activity of the free ligand was increased upon complexation with metal ions; the enhancement in activity can be explained on the basis of chelation theory [29]. Chelation reduces the polarity of the metal ion considerably, mainly because of the partial sharing of its positive charge with donor groups and the possible π -electron delocalization over the whole chelate ring. Chelation not only reduces the polarity of metal ion, but also increases the lipophilic character of the chelate. As a result of this, the interaction between the metal ion and the cell walls is favored, resulting in interference with normal cell processes. This process, in turn, increases the lipophilic nature of the central metal atom, which favors its permeation more efficiently through the lipid layer of the micro-organism thus destroying them more aggressively.

3.8.2. Antifungal Activity

In the case of antifungal activity, the results were compared with the standard drug (Nystatin). The results of antifungal activity of test compounds were found to be somewhat different from their antibacterial activity. All Schiff bases showed activity against fungal species. However, the Cu(II) and Zn(II) complexes (1-6) of these Schiff bases showed much enhanced activity as compared to the uncoordinated compounds. All Schiff bases show high activity against *C. albicans*. Schiff base MPSB is moderate active towards *R. stolonifer*. Moreover, substitution by 3-methoxy group resulted in an increase in activity. The results of antifungal activity of the tested compounds are depicted in Table 1.

The biological activity of the ligands exhibited a marked enhancement on coordination with the metal ions against all fungal strains. However, the metal complexes showed good antifungal activity against *R. bataicola*, *R. stolonifer* and *C. albicans*. It was evident from the data that this activity

significantly increased on coordination. This enhancement in the activity may be rationalized on the basis that their structures mainly possess an additional C=N bond. It has been suggested that the ligands with nitrogen and oxygen donor systems inhibit enzyme activity, since the enzymes which require these groups for their activity appear to be especially more susceptible to deactivation by metal ions on coordination.

3.9. DNA-binding Experiment

3.9.1. Absorption Studies

UV spectroscopic titration is an effective method to examine the binding mode of DNA with metal complexes, since the observed changes of the spectra may give evidence of the existing interaction and its mode [30]. The interaction of titled complexes with DNA was also studied by UV-Vis absorption titration for getting further clues about the mode of interaction and binding strength. The effects of different concentration of DNA on the electronic absorption spectrum of title complexes are shown in Fig. 3. Complex binding with DNA through intercalation usually results in hypochromism and blue shift, due to intercalative mode involving a strong stacking interaction between an aromatic chromophore and the base pairs of DNA [31]. In the present investigation the interaction of titled complexes 1-6 in DMF solutions (10%) with CT DNA have been investigated. Absorption titration experiments of Cu(II) complexes were performed using a fixed complex concentration to which increments of the DNA stock solution were added. The binding of title complexes to duplex DNA led to decrease in the absorption intensities with a small amount of blue shifts in the UV-Vis absorption spectra. This shift effect is associated with the decrease in the energy gap between the highest (HUMO) and the lowest molecular orbitals (LUMO) after the interaction of title complexes to DNA. On the other hand, the coupling π -orbital is partially filled by electrons, thus decreasing the transition probabilities and concomitantly resulting in hypochromism [32].

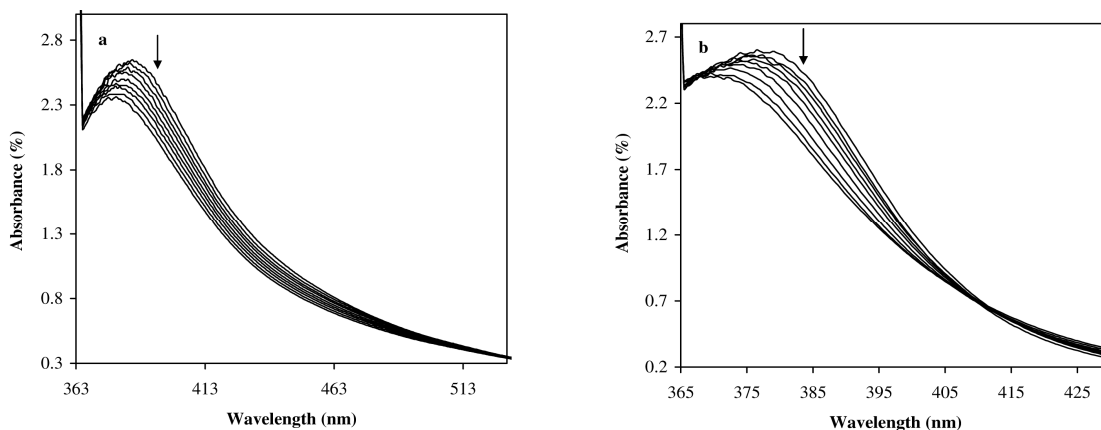


Fig. 3. Absorption spectra of complex a) **2** and b) **4** in the presence of DNA in Tris-HCl buffer upon addition of concentration of CT DNA(0-20 μ M). [complex] = 25 μ M. Arrow shows the absorbance changing upon the increase of DNA concentration.

For metallo-intercalators, DNA-binding is associated with hypochromism and a blue shift in the ligand bands [31]. Fig. 3 shows the absorption spectra of complexes 1-6 in the presence of increasing concentration of DNA. As increasing the concentration of CT DNA, the ILCT transition band of complexes 1 at 383 nm, 2 at 384 nm, 3 at 381 nm, 4 at 377 nm, 5 at 379 nm and 6 at 373 nm exhibits hypochromism of 13.12%, 10.37%, 11.72%, 7.82%, 8.28% and 7.48%, and hypsochromism (blue shift) of 9.5, 8, 6, 4.5, 6.5 and 3 nm, respectively. These spectral

characteristics obviously suggest that complexes 1-6 interact with DNA most likely through an intercalation mode. These significant changes indicate conformational changes and unwinding of DNA base pairs with destabilization of the DNA double helix, which is consistent with DNA intercalation binding mode suggested [33].

In order to further elucidate the binding strength of the complexes, the intrinsic constants K_b were determined by monitoring the changes of absorbance in the ILCT band with increasing concentration of CT DNA. The values of K_b are 2.31×10^4 , 8.73×10^4 , 4.46×10^4 , 3.16×10^4 , 6.03×10^4 and 5.21×10^4 for 1-6 respectively.

3.9.2. Cyclic Voltammetry Studies

The electrochemical investigation of metal-DNA interaction is a useful complement to spectroscopic methods and can provide information about interactions with both the reduced and oxidized form of the metal. The electrochemical potential of a small molecule will shift positively when it intercalates into DNA double helix and, if it is bound to DNA by electrostatic interaction, the potential will shift to a negative direction [34]. Additionally, if more potentials than one present such a shift, a positive shift of E_{p1} and a negative shift of E_{p2} may imply that the molecule can bind to DNA by both intercalation and electrostatic interaction [31].

In the presence of CT DNA, the cyclic voltammograms of the copper(II) and zinc(II) complexes exhibited shifts in the anodic and cathodic peak potentials followed by decrease in peak currents, indicating the interaction existing between the above metal complexes and CT DNA. The drop of the voltammetric currents in the presence of CT DNA can be attributed to diffusion of the metal complex bound to the large, slowly diffusing DNA molecule, explained in terms of an equilibrium mixture of free and DNA-bound complex on the electrode surface [35]. The $E_{1/2}$ values in the presence of CT DNA exhibit positive shifts of 0.027 V for **1**, 0.008 V and 0.051 V for **2**, 0.052V and 0.080 V for **3**.

Complex **2** exhibits the electrochemical behavior upon addition of CT DNA with a positive shift for the cathodic potential E_{pc} [$\Delta E_{pc} = +0.038$ V for Cu(II)/Cu(I), $\Delta E_{pc} = +0.065$ V for Cu(III)/Cu(II) couple] and the anodic potential E_{pa} is shifting to more negative values [$\Delta E_{pa} = -0.064$ V for Cu(II)/Cu(I), $\Delta E_{pa} = -0.011$ V for Cu(III)/Cu(II) couple (Fig. 4A)] followed by a slight increase of current intensity. These shifts of the potentials show that complex **2** can bind to DNA by both intercalation and electrostatic interaction [36]. On the other hand, a positive shift of both the cathodic and anodic potentials is observed for complex **3** [$\Delta E_{pc} = +0.045$ V for Cu(II)/Cu(I), $\Delta E_{pc} = +0.023$ V for Cu(III)/Cu(II) couple and the anodic potential E_{pa} ($\Delta E_{pa} = +0.060$ V for Cu(II)/Cu(I), $\Delta E_{pa} = +0.028$ V for Cu(III)/Cu(II) couple] and for complex **1**, the cathodic potential shift $\Delta E_{pc} = +0.035$ V and the anodic potential shift $\Delta E_{pa} = +0.020$ V is observed for Cu(II)/Cu(I) couple. Thus, the existence of intercalation between **3** and **1** with CT DNA bases may be suggested [36].

It is observed (Table 2) that complexes **4**, **5** and **6** exhibit the same electrochemical behavior upon addition of CT DNA (Fig. 4B). For increasing amounts of CT DNA, the cathodic potential E_{pc} shows a positive shift ($\Delta E_{pc} = +0.036$ V for **4**, $\Delta E_{pc} = +0.016$ V for **5** and $\Delta E_{pc} = +0.034$ V for **6**), marked decreases in the peak current heights and shifts of peak potentials to positive values are observed [31]. The shift in reduction peak potential observed between the reduction of Zn(II)/Zn(I) in complexes **4**, **5** and **6** is indicative for strong intercalative binding.

Table 2. Electrochemical behavior of Cu(II) and Zn(II) complexes in the presence of CT DNA

Complex	Redox couple	$I_{pc}(A) \times 10^{-5}$		E_{pc} (V)		$E_{1/2}$ (V)		ΔE_p (V)		K_{oxd}/K_{red}
		Free	Bound	Free	Bound	Free	Bound	Free	Bound	
1	Cu(II)/Cu(I)	1.18	1.04	-0.897	-0.862	-0.582	-0.555	0.629	0.614	3.91
3	Cu(II)/Cu(I)	3.45	3.19	-0.981	-0.936	-0.576	-0.524	0.804	0.824	5.77
	Cu(III)/Cu(II)	1.52	0.76	-0.136	-0.113	0.084	0.164	0.441	0.390	2.44
2	Cu(III)/Cu(II)	0.81	1.06	-0.019	0.046	0.157	0.165	0.276	0.238	2.86
	Cu(II)/Cu(I)	2.47	2.81	-0.987	-0.949	-0.617	-0.566	0.739	0.765	4.39
4	Zn(II)/Zn(I)	1.10	0.75	-0.978	-0.942	---	---	---	---	4.06
6	Zn(II)/Zn(I)	1.84	1.52	-0.837	-0.803	---	---	---	---	3.76
5	Zn(II)/Zn(I)	1.92	1.53	-0.821	-0.805	---	---	---	---	1.86

The differential pulse voltammograms of the copper complexes **1** and **2** in dimethylformamide solution display irreversible reductive responses (E_{pc} at -0.897 and -0.987 V, respectively) during cathodic scan, attributed to the Cu(II)/Cu(I) couple. Additionally complex **2** shows one cathodic peak in the positive range, $+0.1$ to 0.0 V, the reduction processes Cu(III)/Cu(II) can be observed [Fig.S1A and B(supplementary material)]. The peak potential and current of both complexes are changed in the presence of DNA. K_+/K_{2+} value for the copper complexes suggests that the preferential stabilization of Cu(II) form over Cu(III) and Cu(I) form on binding to DNA. DPV of the complexes as a function of added DNA also indicates a large decrease in current intensity with a small shift in formal potential due to the intercalative interaction of complexes.

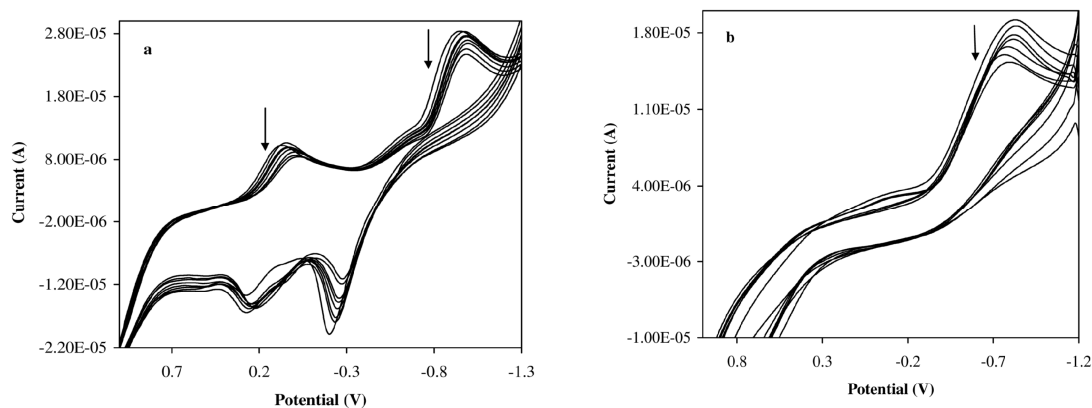


Fig. 4. Cyclic voltammogram in DMF: buffer [mixture 50 mM Tris-HCl/NaCl buffer (pH, 7.2)] (1:2) solution of a) **2** (Scan rate = 0.06 Vs^{-1}) and b) **5** (Scan rate = 0.08 Vs^{-1}) carried out with incremental addition of CT DNA. The arrow mark indicates the current changes upon increasing DNA concentrations.

3.9.3. Viscosity Experiments

To throw further light on the DNA binding mode, viscosity measurements which regarded as the least ambiguous and the most critical test of a DNA binding model in solution and provide stronger arguments for intercalative DNA binding mode. A classical intercalation model results in the lengthening of the DNA helix because base pairs become separated to accommodate the binding ligand, leading to an increase in the viscosity of CT-DNA. In contrast, a partial and/or non-classical intercalation of ligand could bend (or kink) the DNA helix, reducing its effective length and, concomitantly, its viscosity [37]. The effect on the CT-DNA shown in Fig. 5 reveals that the relative viscosity of DNA increased steadily following the order of $2 > 5 > 3 > 6 > 4 > 1$, with an increasing amount of the above compounds. On increasing the concentration of complexes 1-6, the relative viscosity of the DNA increased steadily which is the result of an increase in length of the DNA duplex following intercalation. The results suggest that complexes 1-6 intercalate between the base pairs of CT-DNA, which is also consistent with our foregoing hypothesis.

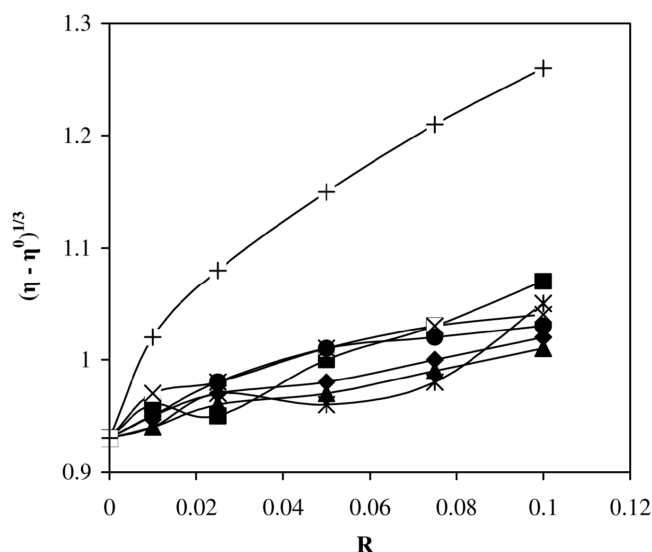


Fig. 5. Effect of increasing amounts of EB (+) and in presence of increasing concentrations of complexes of 1 (▲), 2 (■), 3 (×), 4 (◆), 5 (*), 6 (●) on the relative viscosity of CT-DNA at 30°C. [DNA] = 1.5 mM, R = [complex] / [DNA] or [EB]/[DNA]

4. CONCLUSION

In this work, three new Schiff base ligands and their copper(II) and zinc(II) complexes have been synthesized and characterized. The electronic and magnetic moment data support the four coordination geometry around copper(II) and zinc(II) metal ions. The DNA binding experiments using electronic spectral technique show the hypochromism and red shift at the charge transfer region. Cyclic voltammetric studies have revealed that complex 2 binds to CT DNA by both intercalative and electrostatic interaction, while for 1, 3, 4, 5 and 6 only the intercalative binding mode may be proposed. Viscosity measurement confirms the intercalative binding mode of complexes with DNA. The antibacterial and antifungal data given for the compounds in this paper allowed us to state that the metal complexes generally have better activity than the free ligands.

ACKNOWLEDGMENT

The authors express their sincere thanks to the College Managing Board, Principal and Head of the Department of Chemistry, VHNSN College for providing necessary research facilities. Instrumental

facilities provided by Sophisticated Analytical Instrument Facility (SAIF), IIT Bombay and CDRI Lucknow are gratefully acknowledged. NR thanks the University Grants Commission (UGC), New Delhi for financial assistance

REFERENCES

- [1] K. Krishnankutty, M.B. Ummathur, *J. Indian Chem. Soc.* 83 (2006) 883-887.
- [2] W. Adam, R.T. Fell, V.R. Stegmann, C.R. Saha-Möller, *J. Am. Chem. Soc.* 120 (1998) 708-714.
- [3] M. Tumer, D. Ekinci, F. Tumer, A. Bulut, *Spectrochim. Acta Part A* 67 (2007) 916-929.
- [4] A.K. Patra, S. Roy, A.R. Chakravarty, *Inorg. Chim. Acta* 362 (2009) 1591-1599.
- [5] A.I. Vogel *A Text Book of Quantitative Inorganic Analysis*, 3rd ed., ELBS, Longman, London, 1969.
- [6] M.V. Angelusiu, S.F. Barbuceanu, C. Draghici, G.L. Almajan, *Eur. J. Med. Chem.* 45 (2010) 2055-2062.
- [7] M. Patel, M. Chhasatia, P. Parmar, *Eur. J. Med. Chem.* 45 (2010) 439-446.
- [8] C. Jayabalakrishnan, K. Natarajan, *Transition Met. Chem.* 27 (2002) 75-79.
- [9] A.A. El-Asmy, A.Z. Al-Abdeen, W.M. Abo El-Maaty, M.M. Mostafa, *Spectrochim. Acta Part A* 75 (2010) 1516-1522.
- [10] S.M.E. Khalil, H.S. Seleem, B.A. El-Shetary, M. Shebl, *J. Coord. Chem.* 55 (2002) 883-899.
- [11] U.O. Ozdemir, F. Arslan, F. Hamurcu, *Spectrochim. Acta Part A* 75 (2010) 121-126.
- [12] E. Tas, A. Kilic, M. Durgun, L. Küpecik, I. Yilmaz, S. Arslan, *Spectrochim. Acta Part A* 75 (2010) 811-818.
- [13] N. Padma Priya, S. Arunachalam, A. Manimaran, D. Muthupriya, C. Jayabalakrishnan, *Spectrochim. Acta Part A* 72 (2009) 670-676.
- [14] A. Kulkarni, S.A. Patil, P.S. Badami, *Eur. J. Med. Chem.* 44 (2009) 2904-2912.
- [15] K.R. Surati, B.T. Thaker, *Spectrochim. Acta Part A* 75 (2010) 235-242.
- [16] Z. Chen, Y. Wu, D. Gu, F. Gan, *Spectrochim. Acta part A* 68 (2007) 918-926.
- [17] A. Mukhopadhyay, G. Padmaja, S. Pal, S. Pal, *Inorg. Chem. Commun.* 6 (2003) 381-386.
- [18] A.A.A. Emara, *Spectrochim. Acta, Part A*, 77 (2010) 117-125.
- [19] N. Raman A. Selvan, *J. Coord. Chem.*, 64 (2011) 534-553.
- [20] R.S. Drago, M.J. Desmond, B.R. Corden, K.A. Miller, *J. Am. Chem. Soc.* 105 (1983) 2287-2296.
- [21] M.A. Neelakantan, F. Rusalraj, J. Dharmaraja, S. Johnsonraja, T. Jeyakumar, M. Sankaranarayana Pillai, *Spectrochim. Acta Part A* 71 (2008) 1599-1609.
- [22] M.V. Angelusiu, G.L. Almajan, T. Rosu, M. Negoiu, E.-R. Almajan, J. Roy, *Eur. J. Med. Chem.* 44 (2009) 3323-3329.
- [23] P. Kamalakannan, D. Venkappayya, *Russ. J. Coord. Chem.* 28 (2002) 423-433.
- [24] J. Muller, K. Felix, C. Maichle, E. Lengfelder, J. Strahle, U. Weser, *Inorg. Chim. Acta* 233 (1995) 11-19.
- [25] V.P. Daniel, B. Murukan, B. Sindhu Kumari, K. Mohanan, *Spectrochim. Acta Part A* 70 (2008) 403-410.
- [26] B.J. Hathaway, *Structure and Bonding*, Springer Verlag, Heidelberg, 1973.
- [27] M.S. Sujamol, C.J. Athira, Y. Sindhu, K. Mohanan, *Spectrochim. Acta Part A* 75 (2010) 106-112.
- [28] Z.H. Chohan, A. Scozzafava, C.T. Supuran, *J. Enz. Inhib. Med. Chem.* 17 (2002) 261-266.
- [29] B. Murukan, K. Mohanan, *J. Enzyme Inhib. Med. Chem.* 22 (2007) 65-70.
- [30] H. Chao, W.J. Mei, Q.W. Huang, L.N. Ji, *J Inorg Biochem* 92 (2002) 165-170.
- [31] S. Anbu, M. Kandaswamy, *Polyhedron* 30 (2011) 123-131.
- [32] A.M. Pyle, J.P. Rehmann, R. Meshoyrer, C.V. Kumar, N.J. Turro, J.K. Barton, *J. Am. Chem. Soc.* 111 (1989) 3053-3063.
- [33] N. Raman, A. Selvan, *J. Mol. Stru.*, 985 (2011) 173-178.
- [34] M.T. Carter, M. Rodriguez, A.J. Bard, *J. Am. Chem. Soc.* 111 (1989) 8901-8911.
- [35] S. Tabassum, S. Parveen, F. Arjmand, *Acta Biomaterial* 1 (2005) 677-689.
- [36] G. Psomas, *J. Inorg. Biochem.* 102 (2008) 1798-1811.
- [37] B.D. Wang, Z.Y. Yang, D.W. Zhang, Y. Wang, *Spectrochim. Acta Part A* 63 (2006) 213-219.